

# Electron spin resonance study of surface and oxide interface spin-triplet centers on (100) silicon wafers

Cite as: J. Appl. Phys. **123**, 161582 (2018); <https://doi.org/10.1063/1.5010816>

Submitted: 26 October 2017 . Accepted: 12 January 2018 . Published Online: 31 January 2018

H. Saito, S. Hayashi, Y. Kusano , K. M. Itoh, M. P. Vlasenko, and L. S. Vlasenko 



View Online



Export Citation



CrossMark

## ARTICLES YOU MAY BE INTERESTED IN

[Electron spin resonance identification di-carbon-related centers in irradiated silicon](#)

Journal of Applied Physics **123**, 161592 (2018); <https://doi.org/10.1063/1.5010234>

[Tutorial: Junction spectroscopy techniques and deep-level defects in semiconductors](#)

Journal of Applied Physics **123**, 161559 (2018); <https://doi.org/10.1063/1.5011327>

[Tutorial: Novel properties of defects in semiconductors revealed by their vibrational spectra](#)

Journal of Applied Physics **123**, 161561 (2018); <https://doi.org/10.1063/1.5011036>



## Electron spin resonance study of surface and oxide interface spin-triplet centers on (100) silicon wafers

H. Saito,<sup>1</sup> S. Hayashi,<sup>1</sup> Y. Kusano,<sup>1</sup> K. M. Itoh,<sup>1</sup> M. P. Vlasenko,<sup>2</sup> and L. S. Vlasenko<sup>2</sup>

<sup>1</sup>*School of Fundamental Science and Technology, Keio University, 3-14-1 Hiyoshi, Kohoku-ku, Yokohama 223-8522, Japan*

<sup>2</sup>*Ioffe Institute, Russian Academy of Sciences, St. Petersburg 194021, Russia*

(Received 26 October 2017; accepted 12 January 2018; published online 31 January 2018)

Electron spin resonance (ESR) spectra of surface and interface recombination centers recently observed on (001) silicon wafers, labeled  $P_m$  and KU1, were studied using spin dependent microwave photoconductivity. Both ESR spectra, having the orthorhombic symmetry and spins  $S = 1/2$  and  $S = 1$  for  $P_m$  and KU1, respectively, were observed in the commercially available surface oxidized (001)-Si wafers. Systematic studies on annealing and oxidation conditions for the  $P_m$  and KU1 formation conclude that both ESR spectra arise from the same center that contains the interaction between the two nearest Si dangling bonds on the (001) Si surface. *Published by AIP Publishing.* <https://doi.org/10.1063/1.5010816>

### INTRODUCTION

Defects on silicon surfaces and those at interfaces between silicon and silicon dioxide have been studied extensively for the past 40 years because they can affect the device performance of metal–oxide–silicon field-effect transistors.<sup>1</sup> Electron spin resonance (ESR) spectroscopy is a powerful technique because it provides information about the microscopic structure of defects. Many defects found by ESR at the Si/SiO<sub>2</sub> interface originate from silicon dangling bonds, such as  $P_b$  centers<sup>2</sup> in (111) interfaces and  $P_{b0}$  and  $P_{b1}$  centers in the (001) interface.<sup>3–7</sup> To form a high enough density of  $P_b$  centers for the detection using the traditional ESR technique, the silicon wafers are subjected to high temperature (>800 °C) oxidization for several hours. Moreover, up to 20 silicon samples are packed in single ESR cavity to increase the signal. A typical  $P_b$  density is about  $(1–3) \times 10^{12} \text{ cm}^{-2}$  for a SiO<sub>2</sub> layer with a thickness of 20–120 nm.<sup>4,6</sup>

It has been shown that the thickness of the oxide layer on the silicon surface is about 0.2 nm immediately after immersion in hydrofluoric acid (HF) and reaches ~1 nm during 7 days of oxidization in air at room temperature.<sup>8</sup> The density of paramagnetic surface centers created in the native oxide interfaces is too low to be detected using the normal ESR technique. However, some of such centers can act as recombination centers and can be observed using a special ESR technique using a highly sensitive spin-dependent-recombination (SDR) detection that monitors the change of microwave photoconductivity under magnetic resonance.<sup>9–12</sup> Such a SDR-ESR detection scheme has the sensitivity of a few orders of magnitude higher than that of the conventional ESR method. Applying the SDR-ESR detection scheme, photoexcited spin-triplet ( $S = 1$ ) defects in irradiated silicon<sup>11,12</sup> and in ion implanted layers has been observed.<sup>13–15</sup>

In the previous investigations, we reported the observation of two new ESR spectra of surface centers using the SDR-ESR method: the  $P_m$  center (spin  $S = 1/2$ )<sup>16</sup> and KU1 (spin  $S = 1$ ).<sup>17</sup> Both defects have orthorhombic  $C_{2v}$  symmetry

and exist in the Si/SiO<sub>2</sub> interfaces of commercially available Si (001) wafers. The  $P_m$  center was found at the interface between silicon and native oxide using an isotopically enriched <sup>28</sup>Si sample with a concentration of <sup>29</sup>Si nuclear spins reduced to 0.017%, which led to narrowing of the SDR-ESR lines for proper identification. However, in the naturally abundant silicon containing 4.7% <sup>29</sup>Si isotopes, the lines originating from the  $P_m$  center overlap with lines of the  $P_{b0}$  and  $P_{b1}$  centers, making it impossible to identify the  $P_m$  center independently. The  $S = 1$  KU1 spectrum has a relatively high fine structure splitting, about 85 mT, and is well-observed in any naturally abundant (001) Si wafers having a native SiO<sub>2</sub> layer.<sup>17</sup> It was suggested that the KU1 spectrum arises from the excited triplet state of the  $P_m$  center. The density of  $P_m$  centers is comparable with  $P_b$ -like centers and show spin-dependent recombination to affect the photoconductivity. Therefore, the presence of  $P_m$  centers can affect the performance of semiconductor devices as much as  $P_b$  centers.

In this paper, we perform a systematic study of the  $P_m$  and KU1 centers together using SDR-ESR spectroscopy. Conditions of the  $P_m$  and KU1 spectra formation, including the influence of how the surface SiO<sub>2</sub> are formed, are investigated. The correlating behavior of the  $P_m$  and KU1 spectra and the hyperfine structure lines in the KU1 spectrum allow us to confirm our previously suggested model, which indicated that the same center is responsible for these spectra. Additionally, an observation of the spin flipping in the excited triplet states of the surface recombination centers without irradiation of the ac excitation field for ESR is demonstrated when the externally applied dc magnetic field is tuned to the magnetic fields corresponding to the anticrossing points of the magnetic sublevels of the defects.

### EXPERIMENTAL

The experiments were carried out with commercially produced n-type (001)-oriented silicon wafers, float-zone grown silicon (Fz-Si) with a resistivity of 2500–5000 Ω·cm,

and low resistance ( $\sim 10 \text{ } \Omega\text{-cm}$ ) n- and p-type Czochralski grown silicon (Cz-Si) samples. The n-type Cz-Si samples were subjected to thermal oxidization in dry oxygen after removal of the native  $\text{SiO}_2$  layer by immersing them in 46% water solution of hydrofluoric acid (HF).<sup>8</sup> The thickness of the thermal oxide layer was measured by ellipsometry (Table I).

The concentration of paramagnetic surface centers on silicon is too low to be detected by conventional ESR spectroscopy. However, the ESR spectra of low concentration paramagnetic defects can be obtained using SDR effects when the recombination rate of the photoexcited free carriers and, consequently, the photoconductivity of the sample depends on the spin state of the recombination centers. The ESR spectra can be detected by monitoring the change in microwave photoconductivity through the change in the Q-factor of the cavity. The detailed descriptions of SDR mechanisms and SDR-ESR detection are provided in Refs. 9 and 16–19.

In this work, the SDR-ESR experiments were performed with an X-band (9 GHz) ESR spectrometer (JEOL JES-RE3X). The samples, of size  $3.5 \times 10 \times 0.3 \text{ mm}^3$  with the long edge oriented along  $\langle 110 \rangle$  axis of the crystal, were placed in the cylindrical TE011-mode cavity. The temperature of samples in the range of 20–200 K was adjusted using an Oxford Instruments ESR-900 helium-gas-flow cryostat. The SDR-ESR spectra were observed as the change of microwave photoconductivity of samples under the saturation of magnetic resonance using microwave power in the range of 60–120 mW. Microwave photoconductivity is caused by absorption of the electrical component of the microwave field by photo carriers excited by illumination using a 100-W halogen lamp. A magnetic field modulation of 100 kHz was used, and the second derivative of the absorption signal on the magnetic field was detected. The magnetic field modulation amplitude was about 0.1–0.2 mT for detecting the  $\text{P}_b$ -like spectra with spin  $S = 1/2$  and 2 mT for detecting the triplet  $S = 1$  KU1 spectrum that had larger linewidths.

The lock-in amplifier phase was determined by the sample photoconductivity response to the controlled 100-kHz magnetic field modulation. The lifetime of the photoexcited carriers in pure silicon is comparable to or longer than the modulation period,  $t_m \sim 10^{-5} \text{ s}$ , which requires an almost  $90^\circ$  phase shift of the signal with respect to the field modulation. The lock-in amplifier phase was adjusted for each sample to maximize the signal intensity. The magnetic field applied to samples was calibrated by the well-known isotropic ESR spectra; phosphorus donor electrons ( $S = 1/2$ ,  $g$ -factor = 1.99850, and hyperfine constant  $A = 117.53 \text{ MHz}$ ); and  $\text{Mn}^{2+}$  in  $\text{MnO}$  powder.

## RESULTS AND DISCUSSION

No samples showed the ESR spectra of the surface recombination centers without illumination. Only with the

TABLE I.  $\text{SiO}_2$  layer thickness of the thin film on n-type Cz-Si samples.

Temperature of oxidization ( $^\circ\text{C}$ )	850	850	900	950
Time (min)	17.7	63	170	281
$\text{SiO}_2$ thickness (nm)	1.9	2.6	5.0	10.3

microwave photoconductivity measurements under the electron spin resonance conditions did we observe the SDR-ESR spectra in our silicon samples with native or thermal oxide layers. Typical spectra for (001)-wafer surfaces are shown in Fig. 1. With a wide scan of the magnetic field [Fig. 1(a)], the KU1 (spin  $S = 1$ ) spectrum was observed. A strong broad line at  $B \approx 323 \text{ mT}$  originates from a number of  $\text{P}_b$ -like (spin  $S = 1/2$ ) surface centers, all combined. An expanded central part of the spectra recorded with low modulation amplitudes is shown in Fig. 1(b). In n-type silicon [trace 2 in Fig. 1(b)], phosphorus lines are detected. Note that the KU1 spectrum was not observed in (111) Si wafers where the dominant  $S = 1/2$  spectrum comes from  $\text{P}_b$  centers. The spectra shown in Fig. 1 are identical for all samples and composed of poorly resolved lines of surface  $S = 1/2$  centers.

Figure 2 shows the SDR-ESR spectra detected at two orientations of the n-type 10- $\Omega\text{-cm}$  sample in magnetic fields  $B \parallel [110]$  (a) and  $B \parallel [001]$  (b) together with the calculated positions of the  $\text{P}_{b0}$  and  $\text{P}_{b1}$  spectra for different orientations (lines) using the  $g$ -tensor components summarized in Ref. 6, and for the  $\text{P}_m$  spectrum with parameters taken from Ref. 16. Apparently, the low resolution of spectra at the X-band makes it difficult to identify all peaks completely. However, for some orientations, such as near  $B \parallel \langle 110 \rangle$ , the lines from the orthorhombic  $\text{P}_m$  center were observed. Therefore, in addition to the ESR spectra of the surface dangling bond centers  $\text{P}_b$ ,  $\text{P}_{b0}$ , and  $\text{P}_{b1}$ , the recently reported KU1 and  $\text{P}_m$

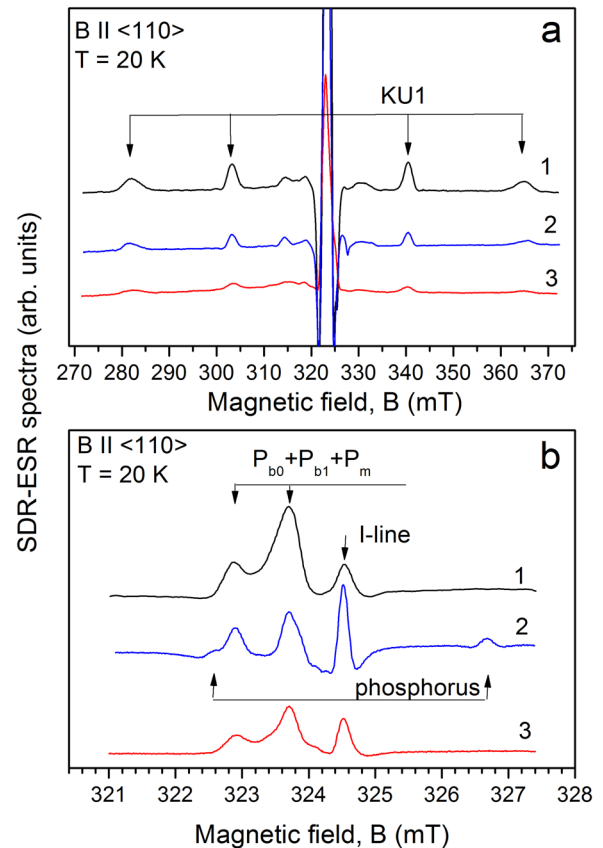


FIG. 1. (a) SDR-ESR  $S = 1$  KU1 spectra and (b) surface spin  $S = 1/2$  spectra detected with an n-type 5000- $\Omega\text{-cm}$  (001) Fz-sample (trace 1), an n-type 10- $\Omega\text{-cm}$  (001) Cz-sample (trace 2), and a p-type 10- $\Omega\text{-cm}$  (001) Cz-Si sample (trace 3) with native oxides that formed naturally in air.

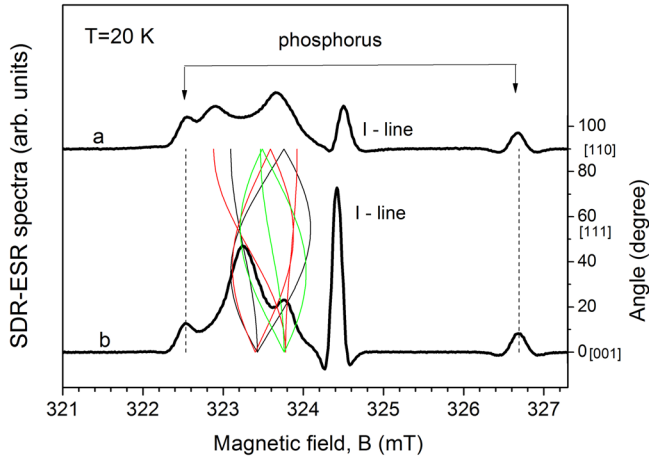


FIG. 2. SDR-ESR spectra detected in n-type 10- $\Omega$ -cm (001) Cz-Si subjected to dry oxidation at 850  $^{\circ}$ C for 17.5 min at  $B||[110]$  (spectrum a) and  $B||[001]$  (spectrum b), and calculated angular dependences for  $P_{b0}$  (black curves),  $P_{b1}$  (green curves) and  $P_m$  (red curves). The microwave frequency was  $f=9.05664$  GHz.

spectra associated with the Si (001) surface with the native or thermally produced  $SiO_2$  layer were observed. The intensities of the KU1 and  $P_m$  spectra are approximately the same for the samples after dry oxidation.

The line labeled I at  $B \approx 324.5$  mT was observed in all the investigated samples at temperatures below 30 K. This line, with the g-factor of  $1.9996 \pm 0.0002$ , was reported in Ref. 16. As can be seen from Fig. 2, this line was slightly anisotropic and shifted to a weaker field of about 0.07 mT when the magnetic field direction changed by 90 $^{\circ}$  from the  $\langle 110 \rangle$  to  $\langle 100 \rangle$  axes. The intensity of the I-line decreased after the removal of the oxide by HF acid. The origin of I-line remains a mystery.

As expected, the removal of the  $SiO_2$  layers by immersing the samples in 46% water solution of HF changed the SDR-ESR spectra. Figure 3 shows the spectra detected with Fz 5000- $\Omega$ -cm Si before and after the removal of the oxide. Here, the widths of the KU1 and  $P_m$  spectral lines decreased after the removal of the  $SiO_2$  layer. This reduction of the linewidths can be attributed to the relaxation of random strains produced by the stress arising from the lattice volume mismatch between the silicon and oxide layers.<sup>20</sup> The intensities of the  $P_{b0}$  and  $P_{b1}$  spectra also decreased by the hydrogen termination of the dangling bond centers.<sup>21</sup> However, the  $P_m$  center, composed of the two nearest interacting Si dangling bonds forming a molecular orbital, was less sensitive to the hydrogen passivation. After keeping the samples in air at room temperature for 7–10 days, all the spectra returned to the original ones, as shown as trace 1 of Fig. 3.

The fine structure splitting  $\Delta B_D$  of the  $S=1$  KU1 spectrum [see Fig. 3(a)] increased from 82.8 to 86.1 mT after the removal of the  $SiO_2$  layer. The fine structure of the  $S=1$  spectra are described by the Hamiltonian

$$H = g\beta S + SDS, \quad (1)$$

where  $\beta$  is the Bohr magneton,  $g$  and  $D$  are the tensors with the components describing the symmetry of the centers.  $D$  is

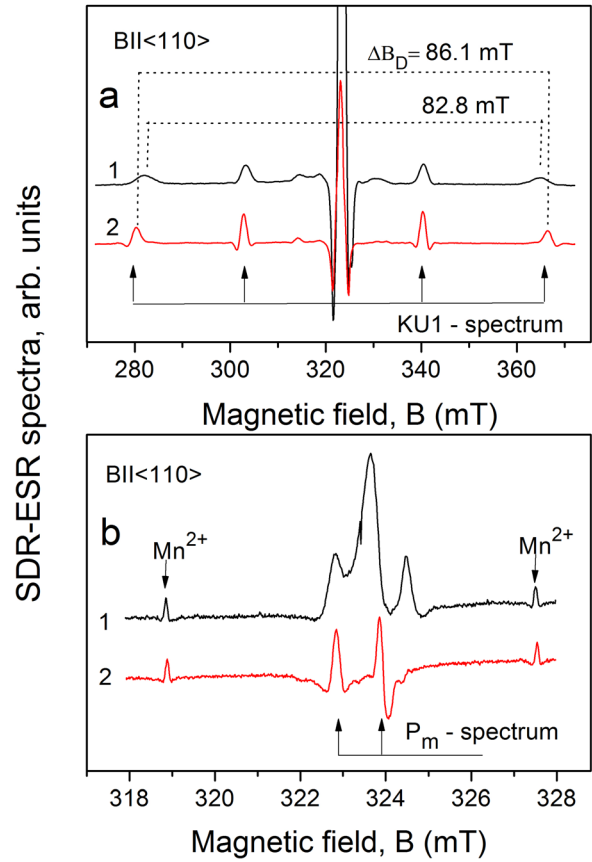


FIG. 3. SDR-ESR detected with the same Fz 5000- $\Omega$ -cm (001) Si sample before (1) and after (2) removal of the surface oxides by HF. Here, the third and fourth  $Mn^{2+}$  lines of the MgO powder were used for calibrating the magnetic field.

the traceless tensor describing the dipole-dipole interaction between the two electrons forming spin  $S=1$ . For  $S=1/2$ , only the first term in Eq. (1) becomes relevant.

The experimental angular dependences of the KU1 and  $P_m$  spectra are shown in Fig. 4 with filled circles. The lines

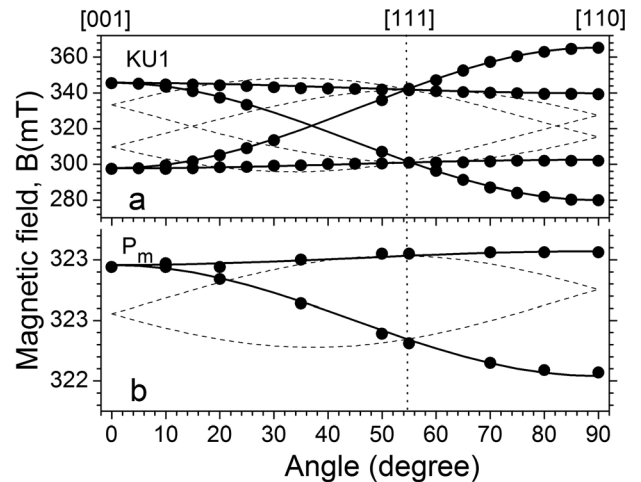


FIG. 4. Angular dependences of the (a) KU1 and (b)  $P_m$  SDR-ESR spectra measured immediately after removal of oxide by HF treatment. Solid and dashed lines represent complete calculated dependences assuming  $C_{2v}$  symmetry. The solid curves are for those centers oriented along two different orthogonal  $\langle 110 \rangle$  axes on the Si (001) surface.

TABLE II. Principal values of  $g$  and  $D$  matrices. Numbers 1, 2, and 3 correspond to the  $[110]$ ,  $[\bar{1}\bar{1}0]$ , and  $[001]$  axes of the Si crystal, respectively.

Spectrum, spin	$g_1$	$g_2$ ( $\pm 0.0002$ )	$g_3$	$D_1$	$D_2$	$D_3$	Fine structure splitting $\Delta B_D$ at $B \parallel [110]$ , mT experiment
				MHz, ( $\pm 2$ MHz)			
P <sub>m</sub> $S = 1/2$	2.0093	2.0029	2.0036	...	...	...	...
KU1 $S = 1$ after HF treatment	2.0060	2.0105	2.0080	$\pm 800$	$\mp 350$	$\mp 450$	86.1
KU1 $S = 1$ with the SiO <sub>2</sub> layer	2.0040	2.0105	2.0080	$\pm 775$	$\mp 347$	$\mp 428$	82.8

show the calculated dependences using the parameters listed in Table II and determined by fitting the calculations with the experimental points. Both spectra were well-described by the orthorhombic  $C_{2v}$  symmetry of the  $g$  and  $D$  tensors. In bulk silicon, there are six equivalent orientations that have  $C_{2v}$  symmetry. However, only two orientations were observed in the experiments; the centers oriented along two orthogonal  $\langle 110 \rangle$  axes on the Si (001) surface, as represented by the solid lines in Fig. 4. The similar symmetry and behavior of the KU1 and P<sub>m</sub> spectra allow us to conclude that both spectra arise from the same surface center containing even or odd numbers of electrons. A microstructural model we propose is shown in Fig. 5. Two dangling Si bonds form the bonding ( $\varphi_a + \varphi_b$ ) and the antibonding ( $\varphi_a - \varphi_b$ ) molecular orbitals occupied by two electrons in the neutral charge state. When two electrons are in a bonding orbital, their spins are antiparallel, giving the total spin  $S = 0$ . Under illumination and recombination of the photoexcited electrons and holes, the two electrons can occupy different ( $\varphi_a + \varphi_b$ ) and ( $\varphi_a - \varphi_b$ ) orbitals with parallel spins forming the metastable triplet  $S = 1$  state responsible for the KU1 spectrum.

The spin  $S = 1/2$  P<sub>m</sub> spectrum may arise from the center containing one or three electrons corresponding to positive or negative charge states, respectively. Here, we suggest a model of a center containing two dangling bonds similar to the case of the A-center (a complex of oxygen + vacancy in silicon)<sup>22,23</sup> giving the  $S = 1/2$  ESR spectrum in the negative charge state. It was found that the intensity of the P<sub>m</sub> and KU1 spectra in p-type silicon were lower compared with that in n-type silicon. This allows us to suggest that the P<sub>m</sub> spectrum arises from the negative charge state. Note that the  $g$ -tensor values of the P<sub>m</sub> center shown in Table II remain the same with and without the SiO<sub>2</sub> layer.

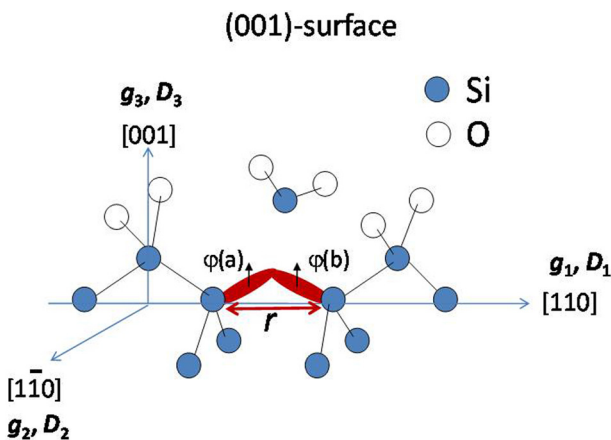
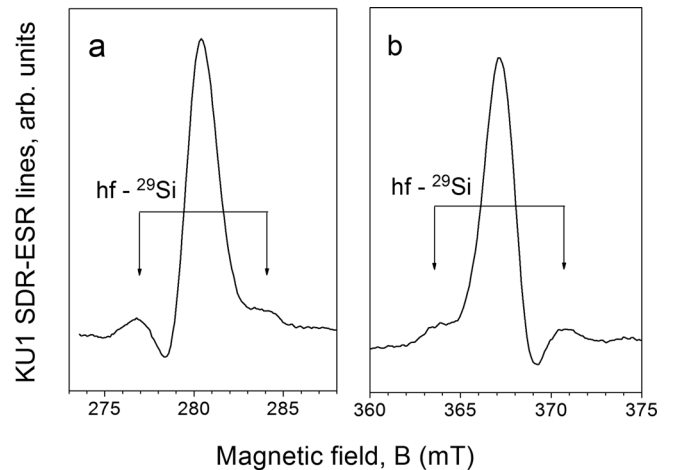


FIG. 5. Microstructure model of the di-Si dangling bond center at the (001) interface.

The maximum fine structure splitting  $\Delta B_D$  of the KU1 spectrum was observed at  $B \parallel [110]$ . This splitting was determined by the  $D_1$  component of  $D$ , depending on the distance  $r$  between the two electrons localized on the dangling bonds of the two nearest Si atoms as  $1/r^3$ . Comparing the distance between the two Si atoms for the excited triplet states of the neutral A-centers (a complex of oxygen + vacancy) in silicon,<sup>24</sup> the distance  $r$  can be estimated as  $\sim 3.60$  Å for the surface center after the removal of the oxide in HF and  $\sim 3.63$  Å for centers having the SiO<sub>2</sub> layer on top. It suggests that the oxide layer imposes mechanical stress, increasing the distance between the two nearest Si atoms to  $\sim 0.03$  Å. Our proposed model predicts the hyperfine ( $hf$ ) interaction between the electrons and the <sup>29</sup>Si nuclei (spin  $I = 1/2$  and abundance 4.7%) that can be located at the two nearest sites. The  $hf$  structure of the KU1 ESR lines was observed and shown in Fig. 6. The relative ratio of  $hf$  line intensity to the central line is  $\sim 0.4$ , approximately two times higher than the  $hf$  interaction with one <sup>29</sup>Si nucleus only. This is consistent with our suggestion that the two equivalent Si atoms exist in the center.

Additional evidence that the KU1 SDR-ESR spectrum arose from the excited triplet state of the proposed microstructure is the observation of microwave photoconductivity change under a scanning magnetic field when the externally applied magnetic field corresponded to the anticrossing points of the magnetic sublevels. Here, no extra energy was needed to go between the two levels, so flipping of the electron spin occurred without the externally applied ac excitation fields. The results are shown in Fig. 7. The energy levels were calculated using the parameters of the spin

FIG. 6. The hyperfine ( $hf$ ) structure of low (a) and high field (b) lines of the KU1 spectrum caused by interaction with <sup>29</sup>Si nuclei occupying the two equivalent nearest-neighbor atomic positions.

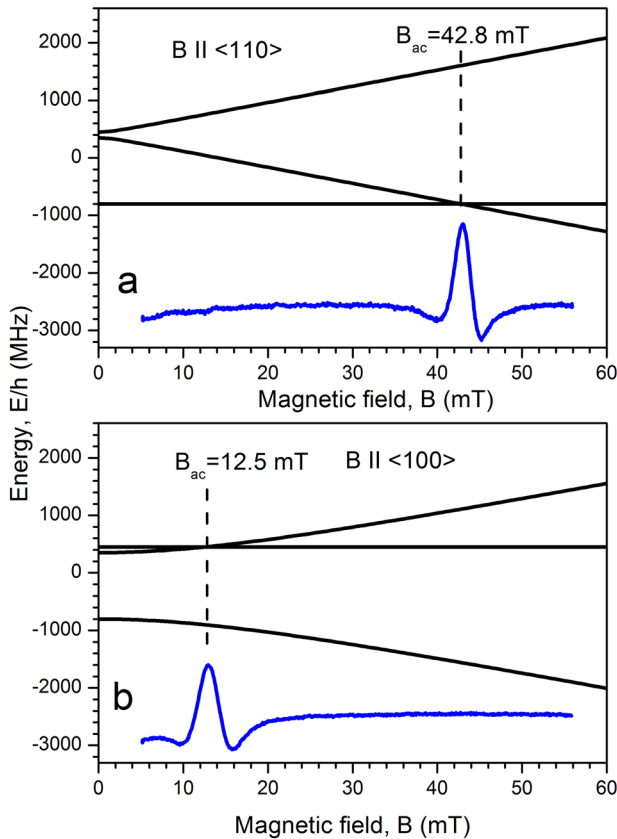


FIG. 7. Energy levels of the KU1 center in magnetic field  $B$  and signals of microwave photoconductivity detected for (a)  $B \parallel \langle 110 \rangle$  and (b)  $B \parallel \langle 100 \rangle$  at  $T = 30$  K.

Hamiltonian listed in Table II for two orientations of the magnetic field corresponding to principal axes of  $\mathbf{g}$  and  $\mathbf{D}$  tensors. The positions of the observed lines of microwave photoconductivity shown in Fig. 7 agree with the calculated values of magnetic fields corresponding to the anticrossing points of the magnetic sublevels of the considered center.

## CONCLUSIONS

Two ESR spectra,  $P_m$  (spin  $S = 1/2$ ) and KU1 (spin  $S = 1$ ), of orthorhombic symmetry arising from the recombination centers localized on an Si (001)-oriented surface with or without a native or thermally produced  $\text{SiO}_2$  layer were investigated using a spin dependent microwave photoconductivity method. Both spectra are sensitive to the mechanical stress imposed by the  $\text{SiO}_2$  layer to the Si surface. The removal the oxide layer by chemical treatment in HF leads to a decrease in the linewidths of both spectra and to an increase in the fine structure splitting for the KU1 spectrum, as determined by the magnetic dipole interaction between the two electrons forming a spin  $S = 1$  center. This shows that the mechanical stress due to  $\text{SiO}_2$  increases the distance between the two interacting electrons with respect to the case where no  $\text{SiO}_2$  layer is present. The mechanical stress also affects the  $g_1$ -component of the KU1 spectrum.

However, the change in the  $P_m$  g-tensor components between with and without  $\text{SiO}_2$  was not observed.

$^{29}\text{Si}$  *hf* structure splitting of the KU1 spectrum was observed, and the analysis concluded that the  $^{29}\text{Si}$  nuclei occupy the two nearest equivalent positions along the  $\langle 110 \rangle$  directions on the (001)-Si surface. Based on this observation, a model of the center responsible for the  $P_m$  and KU1 spectra arising from the two nearest interacting dangling bonds that form bonding and antibonding molecular orbitals was suggested. Moreover, the KU1 spectrum was suggested to arise from the excited triplet states of the neutral  $P_m$  center.

The change in the microwave photoconductivity without a magnetic resonance excitation field was found at the magnetic fields corresponding to the anticrossing points of the magnetic sublevels of the KU1 center. This change in the photoconductivity at the predicted anticrossing field supported the validity of the microstructural model that we proposed for the two centers.

## ACKNOWLEDGMENTS

This work was supported by the JSPS Core-to-Core Program and Spin RNJ. We thank George Watkins for his continuous encouragement in this work.

- <sup>1</sup>P. M. Lenahan and M. A. Jupina, *Colloids Surf.* **45**, 191 (1990).
- <sup>2</sup>Y. Nishi, *Jpn. J. Appl. Phys., Part 1* **10**, 52 (1971).
- <sup>3</sup>E. H. Poindexter, P. J. Caplan, B. E. Deal, and R. R. Razouk, *J. Appl. Phys.* **52**, 879 (1981).
- <sup>4</sup>K. L. Brower, *Semicond. Sci. Technol.* **4**, 970 (1989).
- <sup>5</sup>C. R. Helms and E. H. Poindexter, *Rep. Prog. Phys.* **57**, 791 (1994).
- <sup>6</sup>A. Stesmans and V. V. Afanas'ev, *J. Appl. Phys.* **83**, 2449 (1998).
- <sup>7</sup>M. Jivanescu, A. Stesmans, and M. Zacharias, *J. Appl. Phys.* **104**, 103518 (2008).
- <sup>8</sup>M. Morita, T. Ohmi, E. Hasegawa, M. Kawakami, and M. Ohwada, *J. Appl. Phys.* **68**, 1272 (1990).
- <sup>9</sup>L. S. Vlasenko, M. P. Vlasenko, V. N. Lomasov, and V. A. Khramtsov, *Sov. Phys. JETP* **64**, 612 (1986) [*Zh. Eksp. Teor. Fiz.* **91**, 1037 (1986)].
- <sup>10</sup>R. Laiho, M. M. Afanasjev, M. P. Vlasenko, and L. S. Vlasenko, *Phys. Rev. Lett.* **80**, 1489 (1998).
- <sup>11</sup>M. M. Afanasjev, R. Laiho, L. S. Vlasenko, and M. P. Vlasenko, *Mater. Sci. Forum* **258–263**, 559 (1997).
- <sup>12</sup>L. S. Vlasenko, *Phys. Solid State* **41**, 697 (1999) [*Fiz. Tverd. Tela* **41**, 774 (1999)].
- <sup>13</sup>R. Laiho, L. S. Vlasenko, M. P. Vlasenko, V. A. Kozlov, and V. V. Kozlovski, *Appl. Phys. Lett.* **74**, 3948 (1999).
- <sup>14</sup>P. A. Mortemousque, T. Sekiguchi, C. Culan, M. P. Vlasenko, R. G. Elliman, L. S. Vlasenko, and K. M. Itoh, *Appl. Phys. Lett.* **101**, 082409 (2012).
- <sup>15</sup>D. P. Franke, M. Otsuka, T. Matsuoka, L. S. Vlasenko, M. P. Vlasenko, M. S. Brandt, and K. M. Itoh, *Appl. Phys. Lett.* **105**, 112111 (2014).
- <sup>16</sup>T. Matsuoka, L. S. Vlasenko, M. P. Vlasenko, T. Sekiguchi, and K. M. Itoh, *Appl. Phys. Lett.* **100**, 152107 (2012).
- <sup>17</sup>M. Otsuka, T. Matsuoka, L. S. Vlasenko, M. P. Vlasenko, and K. M. Itoh, *Appl. Phys. Lett.* **103**, 111601 (2013).
- <sup>18</sup>G. A. C. M. Spierings, *J. Mater. Sci.* **28**, 6261–6273 (1993).
- <sup>19</sup>L. S. Vlasenko, *Appl. Magn. Reson.* **47**, 813 (2016).
- <sup>20</sup>K. L. Brower, *Phys. Rev. B* **33**, 4471 (1986).
- <sup>21</sup>K. L. Brower, *Phys. Rev. B* **38**, 9657 (1988).
- <sup>22</sup>G. D. Watkins, J. W. Corbett, and R. M. Walker, *J. Appl. Phys.* **30**, 1198 (1959).
- <sup>23</sup>K. L. Brower, *Phys. Rev. B* **4**, 1968 (1971).
- <sup>24</sup>Y. Kusano, H. Saito, L. S. Vlasenko, M. P. Vlasenko, E. Ohta, and K. M. Itoh, *J. Appl. Phys.* **118**, 245703 (2015).